

The Application of VMM3A Readout for Multi-Grid Neutron Detectors

A. Backis^a, F. Piscitelli^a, D. Pfeiffer^a, J.R.M. Annand^b, M. Aouane^a, K. G. Fissum^a, K. Livingston^b, G. Mauri^c, D. Raspino^c

^a*Detector Group, European Spallation Source ERIC, SE-221 00 Lund, Sweden*

^b*School of Physics and Astronomy, University of Glasgow G12 8QQ, Scotland, UK*

^c*ISIS Facility, Rutherford Appleton Laboratory, Harwell Campus, Oxfordshire OX11 0QX, UK*

Abstract

The T-REX neutron spectrometer at the European Spallation Source will use Multi-Grid Technology, which is a voxelised proportional counter relying on $^{10}\text{B}_4\text{C}$ coatings to detect the scattered neutrons. Measurements of the position dependence of pulse-height and relative detection efficiency of a Multi-Grid prototype of the T-REX spectrometer are presented for two different schemes of signal-processing electronics based on the VMM3A ASIC and CREMAT technology. These measurements, intended to test the suitability of VMM3A for readout of the T-REX Multi-Grid, are compared with Monte Carlo simulations based on the Garfield++ and Geant4 tool kits.

1. Introduction

Multi-Grid (MG) technology for detection of thermal or cold neutrons, originally developed at ILL [1], will be used for the T-REX bispectral chopper spectrometer to be installed at the European Spallation Source (ESS) [2]. MG is a vertical stack of grids, each a rectangular lattice of normal and radial Al blades (Fig.1). The grids form the cathodes of a voxelised proportional counter (VPC), with wires strung vertically through the centres of each voxel providing the anodes. The normal blades are coated at ESS with ^{10}B -enriched (97%) B_4C [3], and neutron capture in this film of B_4C produces ^4He and ^7Li residual nuclei, one of which escapes the film into the VPC gas (Ar- CO_2 in the present case) generating a signal.

This work describes a comparison of signal properties for two alternative schemes to read out the charge collected from the MG electrodes. This was performed using the EMMA thermal neutron beam [4] at the ISIS neutron spallation source in the UK.

*Corresponding Author

Email address: john.annand@glasgow.ac.uk (J.R.M. Annand)

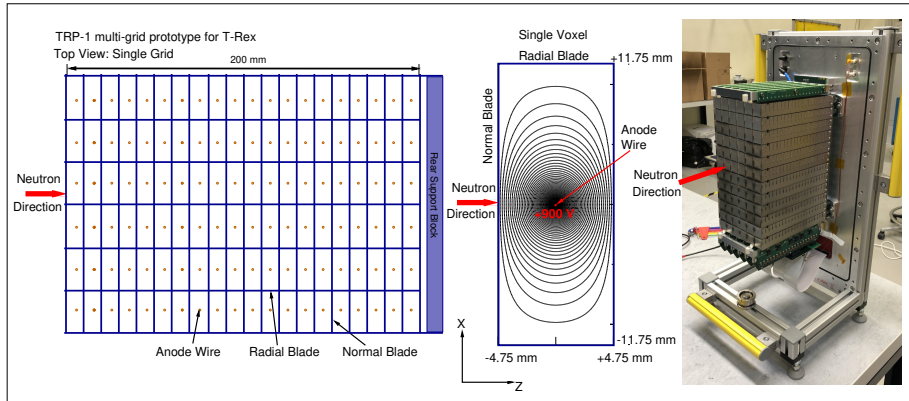


Figure 1: Left: a single grid from the T-REX prototype TRP-1. Middle: a single voxel of the grid showing equipotential contours calculated by Garfield++. Right: a photograph of TRP-1 at ESS with the outer gas enclosure vessel removed, showing the stack of 12 grids.

2. Technical Details

The MG voxel, viewed from the top in Fig. 1, is an elongated rectangle measuring $23.5 \times 9.5 \text{ mm}^2$ in the $x - z$ plane, while it is $23.5 \times 24.0 \text{ mm}^2$ in the $x - y$ plane. When a positive high voltage (HV) is applied to the anode wire, the corners of the voxel experience very low voltage gradients compared to more central regions. This affects the charge collection time, which increases as the neutron-capture position moves from the centre at $x = 0.0 \text{ mm}$ to a corner at $x = \pm 11.75 \text{ mm}$. Neutrons are captured on the normal-blade coatings at $z = \pm 4.75 \text{ mm}$.

T-REX prototype detector TRP-1 was tested. Unlike subsequent T-REX prototypes, this has no internal neutron shielding, such as B_4C coating on the radial blades, but this does not affect charge collection. The absence of capture events on radial blades makes the understanding of the pulse-height response simpler. The coating thickness on the normal blades is $\approx 1 \mu\text{m}$ on the front voxels, rising to $\approx 2 \mu\text{m}$ on the rear voxels. As an important goal here was to compare different electronic readout systems, the same detector was connected to the two sets of electronics based on the VMM3A ASIC and CREMAT technology described in Sec. 2.1.1 and Sec. 2.1.2 respectively.

2.1. Electronics

The major motivation for this work was to test the suitability of read-out electronics based on the VMM3A ASIC for T-REX. VMM3A is used on the Multi-Blade detector [5], employed on three instruments at ESS, and is available in sufficient quantity to instrument T-REX. However, due to relatively slow charge collection in the MG, the maximum pulse-shaping time constant on the front-end pulse amplifier is shorter than optimum for a MG-type VPC. Thus CREMAT

amplifiers with longer shaping times were also tested for comparison. The latter however are not suitable for instrumentation of T-REX, which will contain 60, 88-grid columns of MG, giving a total of 12480 channels to read out. A schematic of the readout electronics is displayed in Fig. 2. TRP-1 has 12 grids (cathodes) and 120 wires, giving 132 channels and 1440 voxels in total. Signal lines attached to the wire and grid electrodes were fed through the gas containment vessel of TRP-1 and connected to either VMM Hybrid or CREMAT cards. With the VMM Hybrid all channels were recorded, while for CREMAT 32 wires and 12 grids were recorded due to a limited supply of this hardware. High voltage was supplied by a CAEN NDT1470 under software control.

In addition to TRP-1 the data acquisition system (DAQ) also accepted the Start Time from the accelerator for time of flight (TOF) determination, the EMMA beam monitor for neutron flux normalisation and optionally a ^3He tube attached to CREMAT electronics for comparison of detection efficiency.

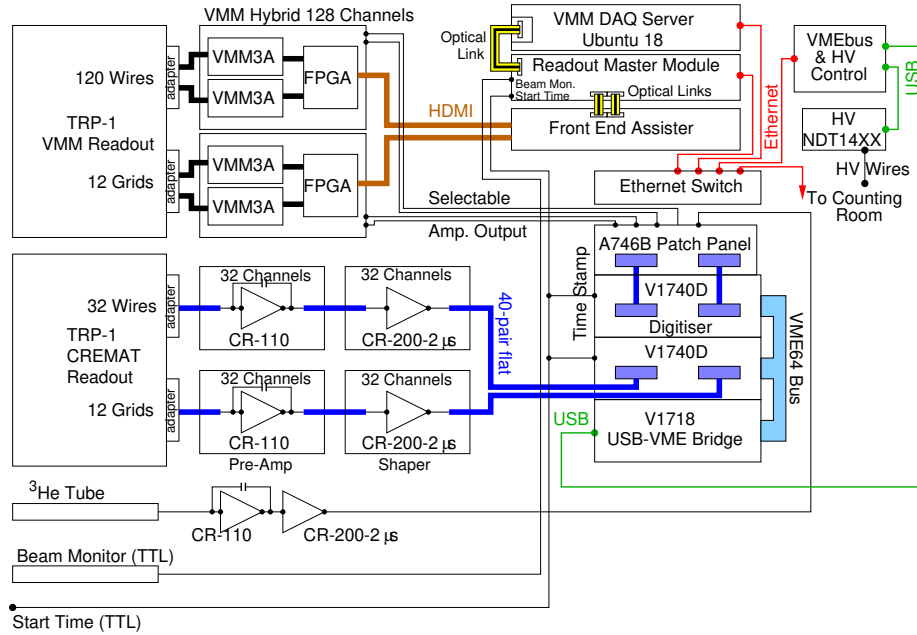


Figure 2: Schematic diagram of the readout electronics. Either VMM hybrids or CREMAT pre-amps were connected to the TRP-1 wires and grids via adapter cards.

2.1.1. VMM3A

VMM3A [6] is a 64-channel ASIC [6, 7], developed at Brookhaven National Laboratory for ATLAS at CERN, and designed to readout Micromegas and sTGC detectors, which are considerably faster than a MG VPC. It is a high density system with fast data transfer capability, suitable for large numbers of readout channels.

Each VMM3A channel contains an analogue section consisting of a charge sensitive preamplifier, a shaping amplifier a discriminator and a peak finder. The gain of the system can be adjusted over a range of 0.5 mV/fC to 16.0 mV/fC, and the peaking time of the shaper can be set to values between 25 ns and 200 ns. Peak pulse height (PH) and trigger time are then digitised on-chip. The pulse peaking time was set to the maximum of 200 ns, which is shorter than optimum for MG detectors, while the gain was set to 3 mV/fC for anode wires and 4.5 mV/fC for cathode grids.

The VMM3A ASICs are integrated into the ‘Scalable Readout System’ [7] developed by the RD51 collaboration. Two ASICs are mounted on a VMM hybrid card, giving a total of 128 channels. The hybrid also mounts a Spartan-7 FPGA which reads the digitised pulse height, time stamp and channel ID from the ASICs and passes the assembled data to the Front End Assistor (FEA) via HDMI cables. On this system the FEA receives LVDS signals, converts to a serial optical standard and sends the data to a Readout Master Module (RMM) via optical fibres. The RMM also receives the TTL start time and BM output, which are incorporated in the data stream and passed to the VMM DAQ Server via optical fibres. Both the FEA and RMM have been developed at ESS.

Low voltage power to the VMM hybrids is supplied by the FEA. The hybrids also mount 00-Lemo ports to which selected signals from the VMM3A amplifiers can be routed under software control. These signals were sent to a CAEN V1740D digitiser [8], which recorded the waveform. Note that the VMM3A pulse-height spectra displayed in this article are derived from the peak pulse height digitised on-chip.

2.1.2. CREMAT

CreMAT amplifiers [9] read out by a CAEN V1740D pulse digitiser [8] are quite flexible to use and convenient for testing small prototypes, but the density of channels is too low for instrumentation of large spectrometers. Charge from the MG electrodes was collected by CR-110 charge-sensitive preamplifiers coupled to CR-200-2 μ s shaper amplifiers. These were mounted on 32-channel PCBs produced at ESS. The pre-amp gain was 1.4 mV/fC, while the shaper gain was 10 followed by a resistive attenuation factor of 6, giving a final gain of 2.3 mV/fC. Attenuation was required to bring the pulse amplitude within the dynamic range of the subsequent pulse digitiser which operated in two modes: either recording the waveform produced by the CREMAT amplifier, or integrating the waveform over a time period of 10 μ s to produce the pulse amplitude. Integration was performed by DPP-QDC firmware from CAEN. Pulse amplitude, time stamp and channel ID were then read from the digitisers by the VME & HV control laptop via the VMEbus and a CAEN V1718 VME-USB bridge.

3. Measurements at EMMA

The TRP-1 prototype was tested at the EMMA beam line of the ISIS spallation neutron source in the UK. Fig. 3 displays a simplified schematic of the test

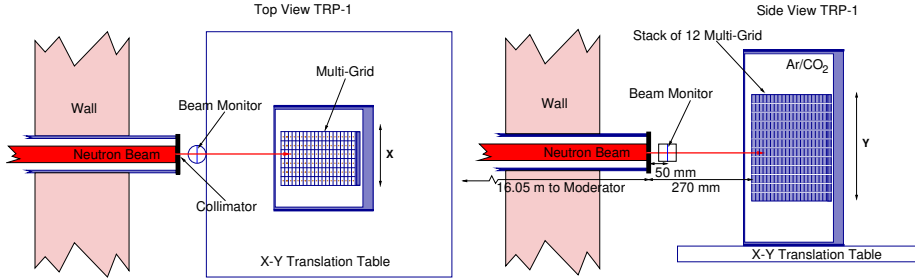


Figure 3: Schematic of the measurement at EMMA, showing the positioning of the TRP-1 multi-grid prototype with respect to the neutron beam line.

setup. The detector was mounted on a $x - y$ translation table and aligned by scanning the direct beam across several voxels to determine the positions where it crossed from one voxel to the next. Beam size was determined by B_4C slits which were set to give beam dimensions of $2.0 \times 0.5 \text{ mm}^2$ in the x and y directions. Direct beam measurements employed a ‘white’ neutron beam which peaked in intensity at $\sim 1 \text{ \AA}$ and extended up to $\sim 4.7 \text{ \AA}$. As TOF was recorded, particular ranges of wavelength could be selected in the offline data analysis. Accumulated neutron intensity during a run was determined from the accumulated proton-beam charge on the spallation target and recorded counts on the 0.25 mm-thick GS1 Li-Glass scintillator Beam Monitor (BM) [10].

Measurements were made with the anode-wire HV ranging from 850 to 1050 V in order to determine the optimum setting. A value of 900 V ensured that the VPC operated well within the proportional-mode voltage range and all electronic components operated well within their linear dynamic ranges. All measured and simulated distributions shown in this article are at an HV of 900 V. Both anode and cathode signals are necessary to determine which voxel has fired. However for brevity only anode-wire distributions are shown, as those from the cathode grids are similar.

To ensure efficient rejection of gamma-ray events, the gamma response of the detector was calibrated by inserting a 2 mm-thick sheet of Cd on the front face of the detector. Cd has an extremely high neutron capture cross section, so that it blocks neutrons, at the same time producing gamma rays from the radiative capture process. These convert to electrons in the materials of the MG detector, mainly by Compton scattering, which produce a small signal in the VPC. The resulting enhanced-gamma, PH spectra were then used to set the discriminator thresholds to minimise the gamma sensitivity of the detector [11].

The neutron beam was scanned in the x direction (horizontal) across the face of a MG voxel. Measurements were made at x coordinates from -13 to $+13$ mm (with respect to the voxel centre), in steps of 1 mm and this was performed for TRP-1 with both VMM3A and CREMAT readout. Samples of recorded waveforms from VMM3A and CREMAT shaping amplifiers are displayed in Fig. 4. The arrival of a pulse triggers the digitiser, setting the time-zero point

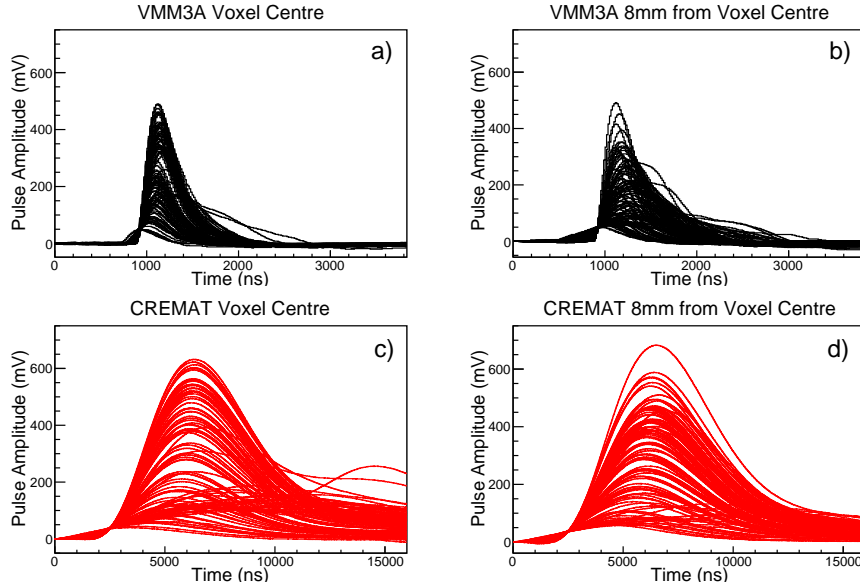


Figure 4: Sample of 100 anode-wire waveforms from VMMA and CREMAT electronics, taken at voxel x coordinates 0.0 and 8.00 mm

on the recorded waveform. Thus delays caused by slow charge collection near the voxel corners were not preserved (see Sec. 4).

Comparison of VMM3A waveforms taken at $x = 0.0$ mm (Fig. 4a) and $x = 8.0$ mm (Fig. 4b) shows that the former has a more sharply defined maximum PH at around 480 mV corresponding to the maximum energy loss of an alpha produced in the neutron capture process. The pulse shapes are also quite similar, while at $x = 8.0$ mm the pulse shapes vary considerably, frequently with extended tails.

With CREMAT, there is little apparent difference in pulse shape at $x = 0.0$ (Fig. 4c) and 8.0 mm (Fig. 4d), while there does appear to be a slightly sharper cut off at maximum PH of around 600 mV for $x = 0.0$ mm.

PH spectra obtained with the VMM3A system are displayed in Fig. 5, where the black-shaded distributions are measurements made with the anode-wire potential set to 900 V. These are compared to the red-shaded, simulated distributions, described in Sec. 4. Both measured and simulated histograms display the summed counts from the front six MG voxels in the direct path of the beam, divided by the integrated counts in the BM. The Li-Glass-scintillator [10] BM (Fig. 3) has a computed (Sec.4) neutron detection efficiency of $\approx 0.6\%$, averaged over wavelengths 0.5 to 4.7 Å, the range employed in the data analysis.

Where the neutron capture (and hence starting position of the ^4He or ^7Li track) is close to the centre of a normal blade ($|x| \leq 3$ mm) the distribution displays a ^4He ‘bump’ at the upper end of the spectrum, which washes out progressively

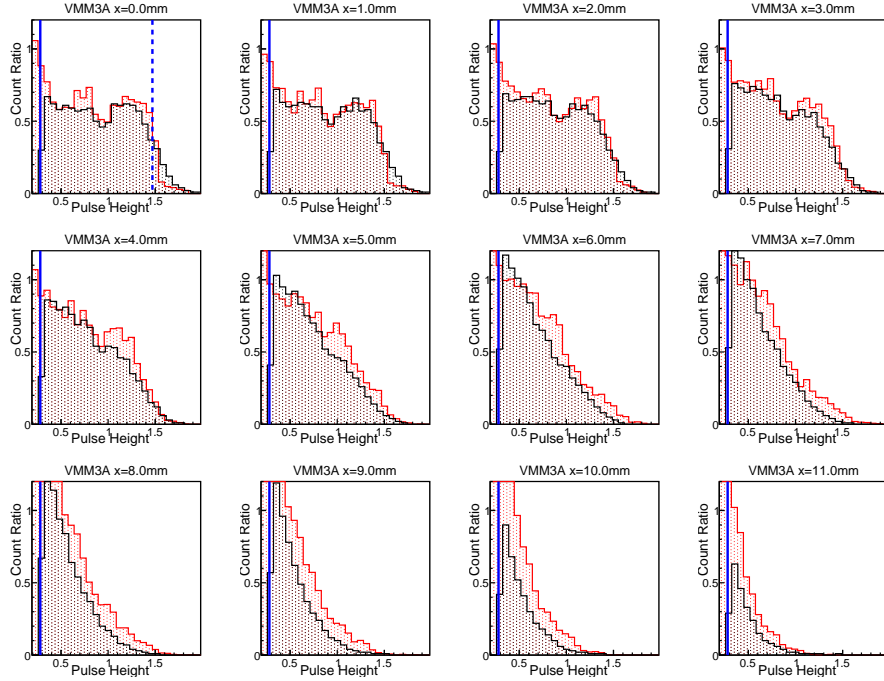


Figure 5: PH spectra obtained for the position scan with VMM3A readout. Pulse-height alignment is described in the text. Count Ratio is the quotient of TRP-1 and BM counting rates. 12 measured spectra (black shading) are displayed for positions $x=0.0$ (top left plot) to $x=11.0$ mm (bottom right) in 1 mm steps. Equivalent Garfield++ simulations are red shaded.

as the capture event moves towards the corner of a voxel. As charge collection becomes slower and more dispersed in time, the short shaping time employed by the VMM3A integrates less of the total charge collected, leading to a loss of PH and PH resolution.

Equivalent PH spectra, taken with the CREMAT readout are shown in Fig. 6 (black-shaded distributions) and compared to simulated red-shaded distributions. Counts were normalised to the BM in the same manner as VMM3A (Fig. 5). The ^4He bump at the high end of the distribution is visible on all spectra, but with a slight decrease in counts towards the voxel corner. The CREMAT amplifier, with a pulse peaking time of $\approx 4 \mu\text{s}$ (a factor 20 larger than the VMM3A), integrates the dispersed charge signals close to a corner more completely.

Since the PH conversion gains differed for VMM3A, CREMAT and the simulation, the PH spectra have been scaled horizontally by constant factors so that the edges of the distributions taken at $x = 0.0$ mm sit at a value of 1.47 units, as shown by the blue dashed lines in Fig. 5 and Fig. 6. 1.47 MeV is the maximum energy of the alpha particle (from the dominant neutron capture channel $n+^{10}\text{B} \rightarrow ^4\text{He} + ^7\text{Li} + \gamma$) when it emerges from the B_4C coating. Thus the PH

scale corresponds approximately to MeV energy. Full blue lines in Fig. 5 and 6 denote the lower integration limit applied to the simulated ratios (see below). This limit is equivalent to the PH threshold applied to the measured data.

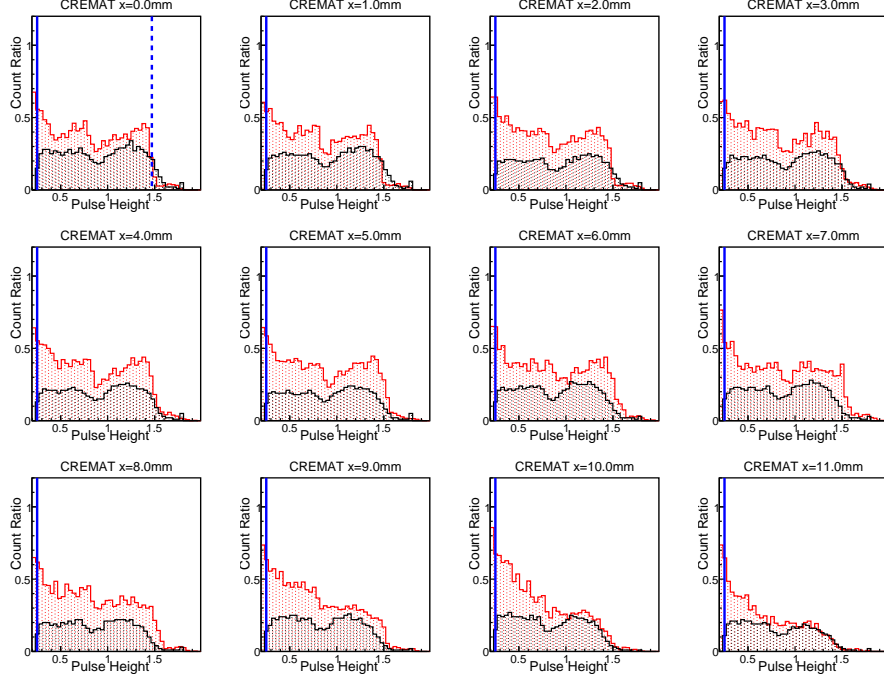


Figure 6: PH spectra obtained for the position scan with CREMAT readout. Axes as in Fig. 5. 12 measured spectra (black shading) are displayed for positions $x=0.0$ (top left plot) to $x=11.0$ mm (bottom right) in 1 mm steps. Equivalent Garfield++ simulations are red shaded.

Integration of PH spectra from threshold upwards gives the ratios of MG/BM counts shown in Fig. 7. It is noticeable that VMM3A ratios are $\sim 10\%$ higher than those from CREMAT for positions $-6 \leq x \leq +6$ mm. One would expect CREMAT, with more complete charge integration, to be better than VMM3A and indeed the simulation predicts slightly higher values for CREMAT. Taking the average ratios for positions $-6 \leq x \leq 6$ mm, the measured value for VMM3a is 86% of the simulated value, while for CREMAT the measured value is 58% of the simulated value.

Thus it seems likely that some CREMAT signals were lost. The incident neutron flux fluctuates due to the pulsed operation of the ISIS proton synchrotron. If the instantaneous rate is sufficiently high, pulse pileup and the internal data processing mechanisms of the V1470D digitiser can lead to losses. In addition the data transfer from digitiser to DAQ control PC has a relatively low bandwidth. VMM3A with much shorter pulses, fast digitisation and high-bandwidth readout is much less prone to such losses.

However the CREMAT distribution shows less loss of efficiency than VMM3A near the corners of a voxel and these general features are reproduced by the simulation.

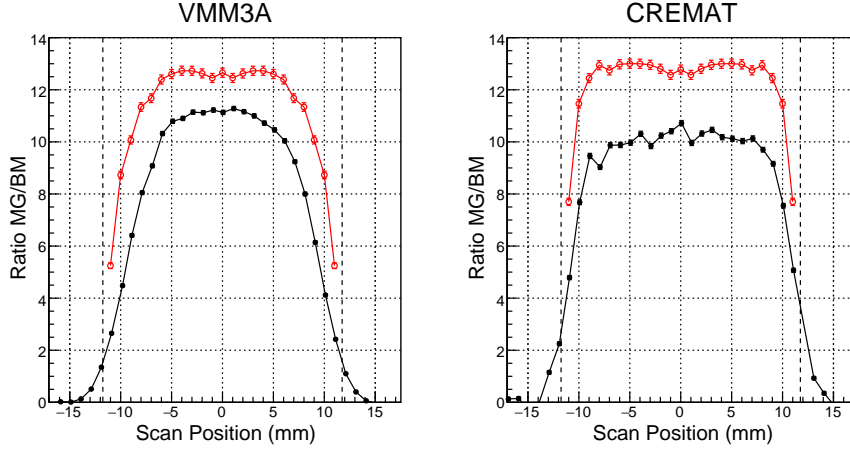


Figure 7: MG/BM counting ratios obtained from the voxel x-scans. Data are shown as filled black circles, while the open red circles show the simulations. The dashed lines denote the edges of the voxel. Error bars, denote statistical uncertainties and the estimated systematic error of the simulation is $\sim 11\%$.

4. Monte Carlo Simulations

A model of the PH response of a MG voxel [12] has been developed using the Garfield++ toolkit [13] in conjunction with Geant4 [14]. ^4He or ^7Li products of neutron capture on ^{10}B , are emitted from the B_4C film coating a normal blade. As they are produced back-to-back only one of the nuclei can reach the chamber gas, while the other stops in the normal blade. The energy of the particle, on reaching the gas, depends on the thickness of B_4C traversed [15], so that the energy and direction were sampled randomly from two-dimensional energy-vs.-angle distributions calculated by a Geant4 model of TRP-1.

The Geant4 model records event-by-event all neutron and gamma interactions in TRP-1 and the BM. The produced ROOT [16] TTree file is then processed to find the energy and direction of the ^4He or ^7Li nuclei emitted from the B_4C film on a normal blade. Energy and polar angle are stored in a two-dimensional ROOT histogram which the Garfield++ model uses to generate randomised starting energy and angle. The present calculations assume $1\ \mu\text{m}$ film thickness for the front voxels of TRP-1, used in the beam scan. The thickness affects the energy loss of particles in the film before they emerge into the chamber gas and the width of the ^4He ‘peak’ at the upper end of the PH distribution. Analysis of the TTree file also records the number of events where a nucleus reaches the chamber gas in the front six in-beam voxels and the integrated counts in the

Li-Glass BM. The ratio of these at $x = 0$ mm is a base value, which is then scaled by the position dependent factors calculated by Garfield++.

In the Garfield++ model the nuclei plough through the detector gas (80/20% Ar/CO₂ mix at STP) producing ionisation and usually they stop in the gas. Energy loss and angle straggling were calculated by SRIM [17] and read in as a look-up table by class TrackSrim of Garfield++. The drift of charge carriers (electrons and ions) induced by the electric field was calculated by Runge-Kutta-Fehlberg integration as implemented by class DriftLineRKF of Garfield++. The accumulated charge as a function of time $Q(t)$, was calculated for electrons and ions on both anode wire and cathode grid.

The $Q(t)$ distributions were then post processed to convolute a ‘transfer function’ ($\mathcal{F}(t)$), to produce a voltage distribution $V(t)$ which can be compared to experiment. A single set of 10^4 ⁴He and 10^4 ⁷Li charge accumulation distributions was calculated for each x value of a position scan and then post processed with either VMM3A or CREMAT pulse shape distributions described by the relation:

$$\mathcal{F}(t) = g \exp(n) \left(\frac{t}{t_p}\right)^n \exp(-t/\tau) \quad (1)$$

For VMM3A parameter $n = 3$ was the number of amplifying stages, $\tau = 67$ ns was the shaping time constant, $t_p = n\tau = 200$ ns was the peaking time and $g = -3.0$ mV/fC was the gain factor, while for CREMAT the parameters were $n = 2$, $\tau = 2$ μ s, $t_p = 4$ μ s and $g = -2.3$ mV/fC.

Fig. 8 shows samples of 150 simulated pulses, calculated with VMM3A pulse shaping parameters at $x = 0.0$ mm (Fig. 8a), $x = 8.0$ mm (Fig. 8b) and CREMAT pulse shaping parameters at $x = 0.0$ mm (Fig. 8c), $x = 8.0$ mm (Fig. 8d). Unlike the experimental situation, time zero t_0 is the point at which the post-capture nucleus emerges from the B₄C layer on a normal MG blade. At $x = 0.0$ mm pulses start very shortly after t_0 and are uniform in shape, while at $x = 8.0$ mm arrival times are spread over several μ s and shapes vary considerably. Both VMM3A and CREMAT simulated waveform amplitudes are 20-25% of the measured waveform amplitudes (Fig. 4), which suggests that the gas gain calculation is too low, but this does not have a significant impact on the relative position dependence of charge collection.

Fig. 9 shows the VMM3A simulations, where the pulses have been shifted in time to start at time $t = 1000$ ns. This mimics the experimental situation (Fig. 4) where the arrival of a pulse triggered the start of the digitisation sequence by the flash ADC. The VMM3A simulations give more of a tail on the pulse than the observation, most visible at $x = 0.0$ mm, where the pulse shape is most uniform. However the VMM3A circuitry does implement ion tail cancellation and this feature is not included in the transfer function convolution (Eq. 1).

For CREMAT charge collection extended up to 10 μ s, while the measurements extend to 16 μ s. Nevertheless the simulation reproduces the pulse shape up to 10 μ s reasonably well.

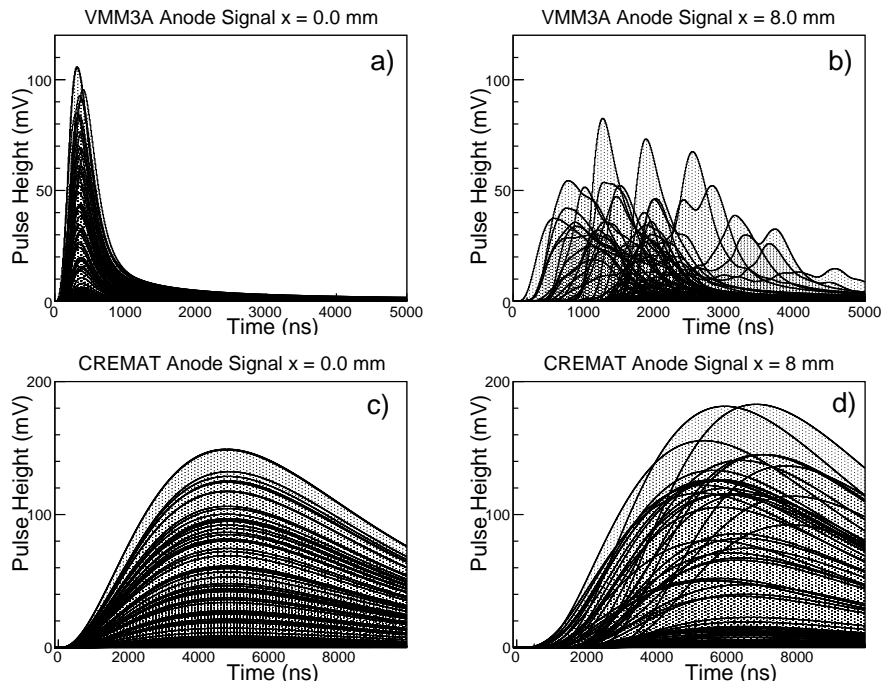


Figure 8: The Garfield++ simulation of pulse forms from VMM3A and CREMAT shaping amplifiers.

As shown in Fig. 7 the simulated MG/BM counting ratios are larger than the measured values. They were calculated for a B_4C thickness of $1.0 \mu\text{m}$ applied to the normal blades of the MG. The maximum uncertainty in thickness is $\sim 0.15 \mu\text{m}$ and at a value of $0.85 \mu\text{m}$ the simulated average central VMM3A efficiency ratio drops from 12.6 to 12.1. This leads to a systematic uncertainty of $\approx 4\%$. The ratio also depends on the computed BM efficiency. The BM had a thickness of 0.25 mm and the composition was as specified for glass type GS1 in Ref.[10]. A threshold of 2 MeV was applied to the simulated PH spectrum to reject gamma-ray events. On the basis of uncertainty in the effective thickness of ${}^6\text{Li}$ in the scintillator, the systematic uncertainty in the computed efficiency ratio is estimated to be $\sim 10\%$. Added in quadrature to the MG B_4C -thickness uncertainty gives a total uncertainty for the ratio of $\pm 11\%$.

5. Summary and Conclusions.

The cuboidal voxels of the MG VPC employed for the T-REX neutron TOF spectrometer at the ESS have low electric field gradients close to the corners. This leads to slow charge collection in these regions, which can reduce the pulse height of the signal and the efficiency for detection of the charged ions produced by neutron capture on ${}^{10}\text{B}$. The position dependence of the pulse-height

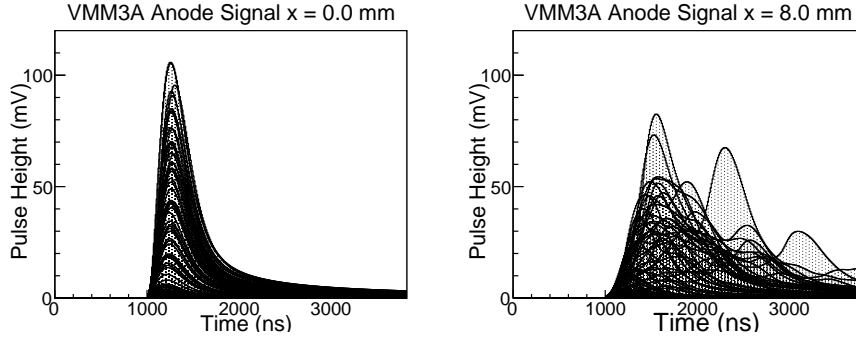


Figure 9: The shifted simulation of pulse forms from the VMM3A shaping amplifier.

response of a T-REX prototype, TRP-1, has been measured using a finely collimated thermal neutron beam at the EMMA test beam line of ISIS. The beam was scanned across a small group of voxels at the front of TRP-1 and the charge collected from the anode wires and cathode grids of the VPC was read out by two alternative sets of electronics based on CREMAT or VMM3A technology.

The major determinant of the pulse-height uniformity across a position scan was the time constant of the shaping amplifier, which effectively sets the integration period of charge collection. A ratio, the quotient of TRP-1 and beam monitor counting rates, was measured. CREMAT, with a pulse peaking time of $4 \mu s$ showed better pulse-height uniformity than VMM3A with a pulse peaking time of 200 ns and this led to less reduction in the ratio at positions close to voxel corners. However VMM3A showed a higher ratio closer to the centre of a voxel.

The pulse-height response and efficiency of TRP-1 have been modelled using a combination of Geant4 and Garfield++. Geant4 gave the probability of neutron capture and the energy distributions of post-capture ions entering the VPC gas, while Garfield++ calculated the time dependence of the charge collected at the anodes and cathode. The model predicts the measured position dependence of pulse-height response quite well for both VMM3A and CREMAT. For VMM3A the measured MG/BM counting ratio was 86% of the predicted value, which has an estimated systematic uncertainty of 11%. However for CREMAT the measurement was only 58% of the predicted value.

Thus there was a significant loss of counting efficiency with CREMAT readout which produced long pulses more prone to pileup effects and also required an external digitiser, which was read out via a fairly low bandwidth link. Pileup was expected to be minimal with the VMM3A, which produced pulses a factor 20 shorter than CREMAT. VMM3A also has fast onboard digitisation and high bandwidth links to output the data, so that counting efficiency losses were expected to be small. In this respect it is ideal for a large spectrometer operating at high rates. The 200 ns peaking time of the VMM3A shaping amplifier is short of optimum and the present Garfield++ simulations predict that a modest increase to 500 ns would bring the position dependence of detection efficiency

very close to the 4 μ s peaking-time (CREMAT) level. This however is not technically feasible with current hardware. With VMM3A readout, the T-REX MG will show drops in efficiency at the horizontal boundaries between voxels, but probably more confined than the gaps in efficiency between the cylindrical ^3He counters installed at several large neutron TOF arrays.

Although VMM3A pulse shaping is not optimum, its high rate capability, fast data transfer and high channel density are ideally suited to T-REX, operating in the high neutron flux environment at ESS. We have concluded that the small losses in detection efficiency, resulting from the short shaping time, are acceptable and that VMM3A-based systems are a suitable platform for T-REX readout.

Acknowledgements

We wish to thank the following for their invaluable assistance:

- the ISIS staff for the efficient provision of the neutron beam at the EMMA facility,
- the technicians of the ESS Detector Group and the University of Glasgow, engaged in the design and construction of Multi-Grid structures and electronics.

The University of Glasgow acknowledge that this work has been generated in collaboration with and through financial support by European Spallation Source ERIC under Contract 325103. Glasgow also acknowledge support from the UK Science and Technology Facilities Council, Grant ST/V00106X/1.

References

- [1] ^{10}B multi-grid proportional gas counters for large area thermal neutron detectors, B. Guérard et al., Nucl. Instr. Meth. A 720, 2013, 116.
- [2] The instrument suite of the European Spallation Source, K.H. Andersen et al., Nucl. Instr. Meth. A 957, 2020, 163402.
- [3] B_4C thin films for neutron detection, C. Höglund et al., J. Appl. Phys. 111, 2011, 104908.
- [4] EMMA test beam line at ISIS. <https://www.isis.stfc.ac.uk/Pages/Instruments.aspx>
- [5] Multi-Blade detector with VMM3a-ASIC-based readout: installation and commissioning at the reflectometer Amor at PSI, F. Piscitelli et al., JINST 19, 2024, 05010
- [6] VMM3a, an ASIC for tracking detectors, G. Iakovidis, J. Phys.: Conf. Ser. 1498, 2020, 012051

- [7] *Rate-capability of the VMM3a front-end in the RD51 Scalable Readout System*, D. Pfeiffer et al, NIM A1031, 2022, 166548.
- [8] *V1740D 64 Channel 12 bit 62.5 MS/s Digitizer supporting DPP-QDC firmware*.<https://www.caen.it/products/v1740d/>.
- [9] Cremat Inc 950 Watertown St, Suite 3 West Newton MA 02465. <https://www.cremat.com/>
- [10] *Neutron Scintillating Glasses Part I*, A.R. Spowart, Nucl. Instr. Meth. 135, 1976, 441.
- [11] *Investigation of gamma-ray sensitivity of neutron detectors based on thin converter films*, A. Kaplanov et al., JINST 8, 2013,10025.
- [12] *Simulation of the T-REX Multi-Grid Detector*, J.R.M. Anand, ESS/T-TREX quarterly meeting, 29th May 2024 <https://indico.ess.eu/event/3524/sessions/7227/attachments/15409/29163/MG.29.05.24.pdf>
- [13] *Garfield++*, H.Schindler et al. <http://garfieldpp.docs.cern.ch/>
- [14] *Geant4 - A Simulation Toolkit*, S. Agostinelli et al., Nucl. Instr. Meth. A 506, 2003, 250. <https://geant4.web.cern.ch/>
- [15] *Analytical modeling of thin film neutron converters and its application to thermal neutron gas detectors*, F. Piscitelli and P. Van Esch, JINST 8, 2013, 04020.
- [16] *ROOT — A C++ framework for petabyte data storage, statistical analysis and visualization*, I. Antcheva et al., Comp. Phys. Comm. 180, 2009, 2499. <https://root.cern.ch>
- [17] *The Stopping and Range of Ions in Matter*, volumes 2 - 6, J.F. Ziegler and J.P. Biersack, Pergamon Press, 1977-1985. <http://www.srim.org>